Tumor Growth Prediction with Hyperelastic Biomechanical Model, Physiological Data Fusion, and Nonlinear Optimization*

Ken C. L. Wong[1], Ronald M. Summers[1], Electron Kebebew[2], and Jianhua Yao[1]

[1] Radiology and Imaging Sciences, Clinical Center, NIH, Bethesda, MD, USA
[2] Endocrine Oncology Branch, National Cancer Institute, NIH, Bethesda, MD, USA

Abstract. Tumor growth prediction is usually achieved by physiological modeling and model personalization from clinical measurements. Although image-based frameworks have been proposed with promising results, different issues such as infinitesimal strain assumption, complicated optimization procedures, and lack of functional information, may limit the prediction performance. Therefore, we propose a framework which comprises a hyperelastic biomechanical model for better physiological plausibility, gradient-free nonlinear optimization for more flexible choices of models and objective functions, and physiological data fusion of structural and functional images for better subject-specificity. Experiments were performed on synthetic and clinical data to verify parameter estimation capability and prediction performance of the framework. Comparisons of using different biomechanical models and objective functions were also performed. From the experimental results on eight patient data sets, the recall, precision, and relative volume difference (RVD) between predicted and measured tumor volumes are 84.85±6.15%, 87.08±7.83%, and 13.81±6.64% respectively.

1 Introduction

The goal of tumor growth prediction is to accurately model the tumor growth process, which is mainly achieved by physiological modeling and model personalization from clinical measurements. If accurate prediction can be achieved from noninvasive measurements, better treatment plan and patient prioritization can be determined, allowing more efficient use of resources. Therefore, image-based tumor growth modeling has been actively researched. In [4], a reaction-diffusion equation was used with a linear mechanical model to simulate brain tumor growth. By combining magnetic resonance images and diffusion tensor images, realistic tumor growth can be simulated. In [6], a reaction-advection-diffusion equation was proposed to model gliomas growth, with the advection term modeling the mass effect. The model personalization was achieved by adjoint-based partial-differential-equation-constrained (PDE-constrained) optimization. In [3], kidney tumor growth was modeled by a reaction-diffusion equation and a linear mechanical model, and the volume-based objective function was minimized by a hybrid optimization method. In [9], by using a similar model and optimization approach in [6], a multimodal framework was proposed to combine images of computed tomography (CT) and positron emission tomography (PET) for pancreatic tumor growth prediction.

P. Golland et al. (Eds.): MICCAI 2014, Part II, LNCS 8674, pp. 25–32, 2014.

Although these frameworks are promising, different issues may limit the prediction performance. For simplicity, most frameworks use linear stress-strain relation and strain-displacement relation. In continuum mechanics, linear strain-displacement approximation should only be used when deformation is less than 5% [7], which is usually not the case for tumor growth. Furthermore, most biological tissues should be modeled as hyper-viscoelastic materials [5]. For parameter estimation, [6] and [9] formulated the problem as adjoint-based PDE-constrained optimization, whose formulations are very complicated and analytical derivatives of the model and objective function are required. Such an approach is not suitable for more complex models, and may limit the choices of better objective functions. Moreover, except [9], only structural but not functional information was utilized, which may limit the patient-specificity of the results.

Therefore, we propose a framework comprising a reaction-diffusion equation and a hyperelastic biomechanical model for pancreatic tumor growth prediction. Adopting the way of incorporating CT and PET images in [9], a gradient-free nonlinear optimization algorithm is used for the model parameter personalization [10]. Using this framework, more complicated objective functions can be studied, and we propose an objective function which accounts for both the mean-squared errors (MSE) of intracellular volume fractions (ICVF) and the volume differences between simulations and measurements. Experiments were performed on synthetic data to verify the parameter estimation capability, and on clinical data for the prediction performance. Comparisons of using different biomechanical models and objective functions were also performed.

2 Methodology

2.1 Physiological Data Fusion with Reaction-Diffusion Equation

To model tumor invasion and proliferation, a reaction-diffusion model is used:

$$\frac{\partial \theta}{\partial t} = \operatorname{div}(\mathbf{D}\nabla\theta) + \rho\theta\,(1-\theta) \tag{1}$$

where $\theta \in (0,1)$ represents the ICVF, which is equivalent to the number of cells (N) divided by the maximum cell capacity (K). ICVF can be computed from dual-phase CT images to provide physiologically meaningful information for model personalization. $\mathbf{D}$ is the anisotropic diffusion tensor, which is a diagonal matrix with components D_x, D_y, and D_z regardless of the tissue structure. ρ is the proliferation rate computed from PET with fluorodeoxyglucose (FDG-PET). The first and second term of (1) account for tumor invasion and cell proliferation respectively. This equation is solved using a Galerkin finite element method (FEM) [2].

Computing Intracellular Volume Fractions from CT Images. To acquire contrast-enhanced CT images, iodine-based contrast agent is injected to the blood vessel, which causes greater absorption and scattering of x-ray radiation in the target tissue, and results in contrast enhancement [1]. As the enhancement of tissue is related to the volume of the extracellular space [8], ICVF (θ) of the tumor can be computed as [9]:

$$\theta = 1 - \frac{HU_{\text{post\_tumor}} - HU_{\text{pre\_tumor}}}{HU_{\text{post\_blood}} - HU_{\text{pre\_blood}}}(1 - Hct) \tag{2}$$

where $HU_{\text{post\_tumor}}$, $HU_{\text{pre\_tumor}}$, $HU_{\text{post\_blood}}$, and $HU_{\text{pre\_blood}}$ are the Hounsfield units of the post- and pre-contrast CT images at the segmented tumor and blood pool (aorta) respectively. Hct is the hematocrit, which can be obtained from patient blood samples. Therefore, the ICVF of the tumor is computed using the ICVF of the blood (Hct) as a reference.

Computing Proliferation Rates from FDG-PET. Energy provided to tissue can be divided into two parts, one for maintaining the existing cells, and another for creating new cells [12]. Therefore, the incoming energy (B) can be represented as:

$$B = B_c K\theta + E_c K\frac{\partial \theta}{\partial t} \tag{3}$$

where B_c and E_c are energies required to maintain and create a cell respectively. By neglecting the invasion part in (1), we substitute $\frac{\partial \theta}{\partial t} = \rho\theta\,(1-\theta)$, and (3) becomes:

$$\rho = \frac{\alpha SUV - \beta\theta}{\theta(1-\theta)}; \quad \text{with } \alpha SUV = \frac{B}{E_c K} \text{ and } \beta = \frac{B_c}{E_c} \tag{4}$$

where SUV is the standardized uptake value computed from FDG-PET, which indicates metabolic activities. $\alpha > 0$ is an unknown scale to be estimated, and $\beta \approx 0.02$ day^{-1} [12]. $B = \alpha E_c K SUV$ indicates that the incoming energy (B) is proportional to SUV. Therefore, the proliferation rate (ρ) can be approximated from PET and ICVF images at measured time points. With (1), (2), (4), physiologically meaningful quantities can be computed from CT and PET and combined for better patient-specificity.

2.2 Hyperelastic Mechanical Model for Mass Effect

For simplicity, most image-based model personalization frameworks use linear elasticity to approximate mass effect. Nevertheless, infinitesimal strain assumption should only be made for very small deformation ($< 5\%$), which is usually not the case for biological tissue. Furthermore, nonlinear constitutive law is required for enforcing tissue incompressibility in large deformation [7]. Therefore, for better physiological plausibility, we use the modified Saint-Venant-Kirchhoff constitutive law [7]:

$$\psi(\boldsymbol{\epsilon}) = \frac{1}{2}\lambda(J-1)^2 + \mu \mathrm{Tr}(\bar{\boldsymbol{\epsilon}}^2) \tag{5}$$

where J is the determinant of the deformation gradient tensor $\mathbf{F}$, and $\bar{\boldsymbol{\epsilon}}$ is the isovolumetric part of the Green-Lagrange strain tensor $\boldsymbol{\epsilon} = \frac{1}{2}(\mathbf{F}^{\mathrm{T}}\mathbf{F} - \mathbf{I})$. The first and second term of (5) account for the volumetric and isochoric elastic response respectively, and thus λ and μ are the bulk and shear modulus respectively. In our model, the tumor and its surrounding tissue have different mechanical parameters.

To simulate mass effect, as the deformation rate is slow for tumor growth, the static equilibrium equation is used to relate the ICVF (θ) with the mechanical model:

$$\mathrm{div}(\boldsymbol{\sigma}) + \mathbf{f}_b = 0; \;\; \mathbf{f}_b = -\gamma\nabla\theta \tag{6}$$

where $\boldsymbol{\sigma}$ is the Cauchy stress tensor, $\mathbf{f}_b$ is the body force, and γ is the unknown force scale to be estimated. With (5) and (6), the total-Lagrangian formulation can be derived and implemented using FEM [2].

2.3 Gradient-Free Nonlinear Optimization

The model personalization is achieved by parameter estimation. The simulation with model parameters $\mathbf{x}$ is rasterized into an ICVF image by using the CT image at the same time point as a reference, and then the following objective function is computed:

$$f(\mathbf{x}) = w_{\mathrm{MSE}}\,\mathrm{E}\left[\left(\bar{\theta} - \theta(\mathbf{x})\right)^2\right] + w_{\mathrm{VD}}\,(1 - recall + 1 - precision); \qquad (7)$$
$$recall = TPV/V_{\mathrm{m}};\;\; precision = TPV/V_{\mathrm{s}}$$

where TPV is the true positive volume, the overlapping volume between the simulated tumor volume (V_{s}) and the measured (segmented) tumor volume (V_{m}). $\bar{\theta}$ and $\theta(\mathbf{x})$ are the respective measured and simulated ICVF within TPV. Therefore, the objective function accounts for both the ICVF mean-squared error and volume difference, and w_{MSE} and w_{VD} control their respective contributions.

As the objective function is complicated and its gradient is difficult to derive analytically, gradient-free direct search methods which make few assumptions about the objective function should be used. Therefore, the subplex method (SUBPLEX) is adopted [10], which is a generalization of the Nelder-Mead simplex method (NMS). A simplex in n-dimensional space is a convex hull of $n + 1$ points, for example, a triangle in 2D. In NMS, a simplex moves through the objective function space, changing size and shape, and shrinking near the minimum. SUBPLEX improves NMS by decomposing the searching space into subspaces for better computational efficiency. With this algorithm, the model personalization can be performed with intact model nonlinearity.

Because of the limitation of the measurements, not all parameters can be estimated. Experiments on synthetic data show that α and β cannot always be separated, thus we adopted $\beta \approx 0.02$ day^{-1} from [12]. For the mechanical parameters, force and stiffness are theoretically inseparable for static analysis, as any proportional force and stiffness produce the same deformation. As the stiffness of pancreatic tissue and tumor is more well studied than the growing force, we adopted the stiffness parameters from [11], with μ_{tissue} = 1 kPa, μ_{tumor} = 5 kPa, and $\lambda_{\mathrm{tissue}} = \lambda_{\mathrm{tumor}}$ = 5 kPa. Therefore, the parameters to be estimated are $\mathbf{x} = \{D_x, D_y, D_z, \alpha, \gamma\}$.

3 Experiments

The proposed framework and two other frameworks were tested on synthetic and clinical data, to study the differences between using linear and nonlinear biomechanical models, and between with and without ICVF. The tested frameworks are:

- **Nonlinear mean-squared error (MSE) and volume difference (VD) (N-MSEVD)**: the proposed framework with nonlinear biomechanics (5) and w_{MSE} = w_{VD} = 1.
- **Linear MSE and VD (L-MSEVD)**: same as N-MSEVD but using Hooke's law (linear mechanical model) [2]. The Young's moduli of tissue and tumor are 1 and 5 kPa respectively. Poisson's ratios = 0.45 for linear model incompressibility.
- **Nonlinear VD (N-VD)**: same as N-MSEVD but only the volume difference is considered in the objective function (i.e. w_{MSE} = 0 and w_{VD} = 1).

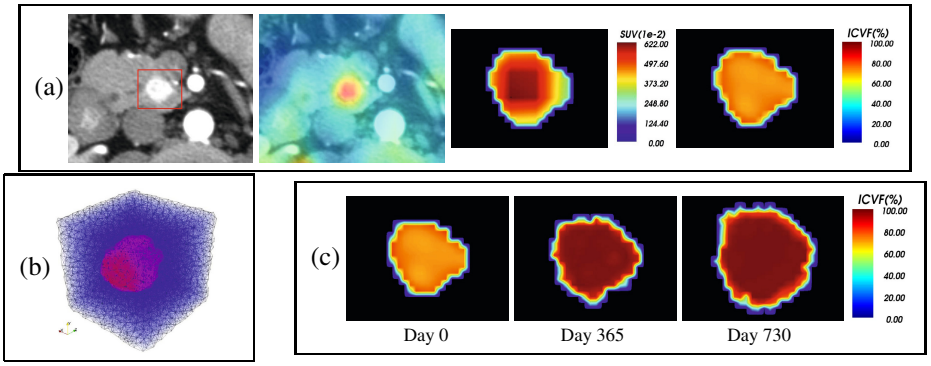

Fig. 1. (a) Post-contrast CT, registered PET-CT, and the computed SUV and ICVF of the tumor (red box). (b) FEM mesh of a tumor (red) and its surrounding tissue (blue). (c) Ground-truth ICVF at three time points of a set of synthetic data ($\alpha = 3$ mm^3/g/day).

3.1 Experimental Setups

In each experiment, measurements at three time points were required. Simulation was performed on the mesh at the first time point, with the ICVF and SUV images providing the initial conditions and proliferation rates in (1) respectively. This simulation was rasterized and compared with the measured ICVF and tumor volume at the second time point to evaluate the objective function for parameter estimation. Prediction was performed by simulating the tumor growth using the personalized parameters, with the mesh, ICVF, and SUV at the second time point. The prediction performance was evaluated using the measurements at the third time point.

To compute ICVF from images, the pre- and post-contrast CT at the same time point were registered using deformable B-spline registration. The tumors were segmented by a semiautomatic level-set algorithm from the post-contrast CT images. For each data set, by using the segmented tumor at the first time point as a reference, PET images and segmented tumors at other time points were registered using rigid registration to preserve the sizes of the tumors, and the corresponding SUV and ICVF were computed (Fig. 1(a)). Linear tetrahedral FEM meshes (3.2 to 4.5×10^4 elements) were built from the segmented tumors and their surrounding tissue (Fig. 1(b)).

3.2 Synthetic Data

We studied the parameter estimation capability using synthetic data. Using the mesh, SUV, and ICVF images of a patient at the first time point (Day 0, Fig. 1(a),(b)), the second time point (Day 365) was simulated with the ground-truth model parameters using the proposed model (Table 1). This FEM simulation was rasterized to an ICVF image (Fig. 1(c)), which was used as the input to the experiments. The estimated parameters were then used to predict the tumor at the third time point (Day 730) and compared with the simulated ground truth. Ground truths with $\alpha = 2.5, 3, 3.5$, and 4 mm^3/g/day were simulated to study the prediction performance at different growth rates. The same initial parameter values were used in all experiments.

Table 1. Synthetic data. Estimated parameters, and the ICVF root-mean-squared error (RMSE), recall, precision, and relative volume difference (RVD)

4 cases	D_x,D_y,D_z(mm^2/day,10^{-3})			γ(kPa)	RMSE(%)	Recall(%)	Precision(%)	RVD(%)
Ground truth	0.50	1.00	0.00	2.00	-	-	-	-
N-MSEVD	0.51±0.01	0.95±0.10	0.09±0.12	1.98±0.04	1.88±1.96	98.81±2.15	97.14±2.71	2.05±2.83
L-MSEVD	0.45±0.14	1.10±0.14	0.02±0.01	4.51±0.10	3.16±2.50	95.26±3.60	97.88±2.03	2.82±3.86
N-VD	0.31±0.20	0.67±0.42	0.22±0.16	1.94±0.09	4.02±2.04	95.02±6.42	96.31±1.83	4.75±5.37

α(mm^3/g/day)								
Ground truth	2.50	3.00	3.50	4.00	N-MSEVD	2.50	3.28	3.23	4.02
L-MSEVD	2.50	2.88	2.96	5.00	N-VD	3.24	3.26	3.37	4.97

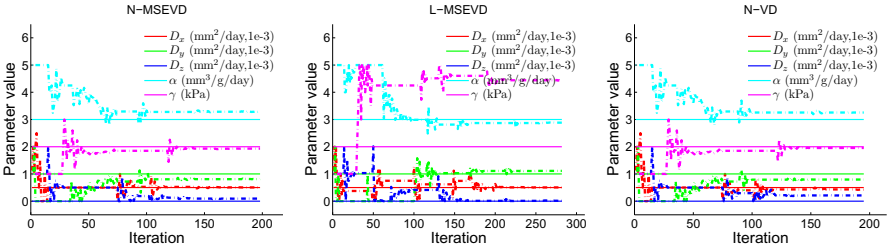

Fig. 2. Synthetic data. Parameter estimations on a set of synthetic data ($\alpha = 3$ mm^3/g/day), with solid lines representing the ground truth values.

Table 1 shows the ground truth and estimated parameters, and also the prediction performance, with RVD $= |V_s - V_m|/V_m$. As the input ICVF data were corrupted by rasterization error, the parameter estimations were nontrivial, and global convergence was not guaranteed. The proposed N-MSEVD framework has the best parameter estimation and prediction performance, as it has the same model as the ground truth and also the complementary measurements in the objective function. The force scaling parameters (γ) estimated by the L-MSEVD framework deviate the most from the ground truth to compensate the difference in the mechanical model. The N-VD framework which does not consider ICVF has the worst estimation and prediction performance.

Fig. 2 shows the parameter evolutions during optimizations. The N-MSEVD and N-VD frameworks are similar in the early iterations (< 100) because of the use of the same model, but the difference becomes larger in the later refinements because of the difference in the objective functions. The L-MSEVD framework evolves more differently than the others, especially for the force scaling parameter. These observations show the importance of using a proper model and complementary measurements.

3.3 Clinical Data

Images from eight patients (five males and three females) with diagnosed pancreatic neuroendocrine tumors were used. The average age and weight of the patients at the first time point were 49.6±13.2 years and 84.9±17.8 kg respectively. Each set of data has three time points of dual-phase CT and FDG-PET images spanning three to four years, and the pixel sizes are less than $0.94 \times 0.94 \times 1$ mm^3 and $4.25 \times 4.25 \times 3.27$ mm^3 respectively. The same initial parameter values were used in all experiments.

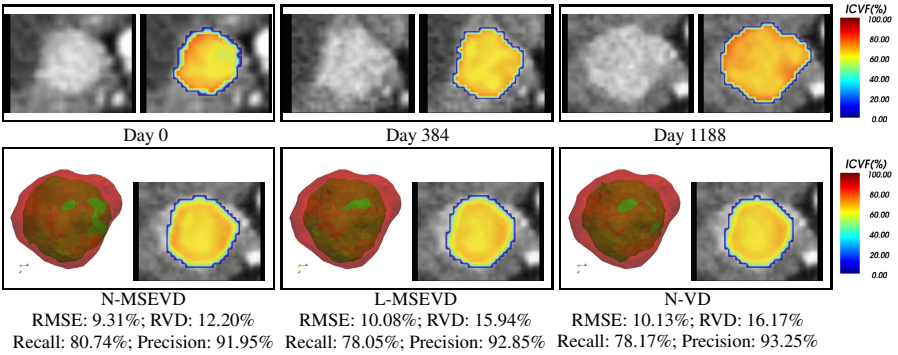

Fig. 3. Clinical data. Top: CT and ICVF at three time points. Bottom: prediction at the third time point, with the measured (red) and predicted (green) tumors superimposed.

Fig. 3 visualizes the results of a patient. In all frameworks, the predicted tumor sizes in the horizontal direction do not match the segmented tumor at the third time point. This is because there is no obvious change along the corresponding direction from the first to the second time point, and thus the estimated parameters cannot account for the change at the third time point. In this example, the proposed N-MSEVD framework has the closest predicted ICVF to the measurements, and also has better volume overlapping with the segmented tumor than the other frameworks, while the L-MSEVD and N-VD frameworks have similar performance.

Table 2. Clinical data. Estimated parameters, and the ICVF root-mean-squared error (RMSE), recall, precision, and relative volume difference (RVD).

8 patients	D_x, D_y, D_z(mm^2/day,10^{-3})			α(mm^3/g/day)	γ(kPa)	RMSE(%)	Recall(%)	Precision(%)	RVD(%)
N-MSEVD	1.39±1.65	0.77±1.01	0.10±0.16	0.31±0.46	0.80±0.85	10.92±1.78	84.85±6.15	87.08±7.83	13.81±6.64
L-MSEVD	1.75±1.53	0.97±1.02	0.34±0.63	0.24±0.32	0.65±1.10	12.05±3.02	83.85±7.46	87.67±8.36	14.81±9.79
N-VD	1.49±1.53	0.83±0.98	0.09±0.17	0.20±0.24	1.23±2.16	11.32±1.47	83.29±6.13	88.45±7.87	13.27±8.73

Table 2 shows the statistics of the estimated parameters and the corresponding prediction performance. The prediction capabilities were evaluated through comparing the personalized simulations with the measurements at the third time point. The small estimated values of the model parameters are consistent with the slow growth of the tumors. The proposed N-MSEVD framework has the best ICVF RMSE and recall, while the N-VD framework has the best precision and RVD. In fact, all frameworks have similar prediction performance, as the differences among the frameworks are subtle with slow tumor growth. Although it is difficult to select the best framework because of this limitation, the high prediction performance shows that the results are promising.

4 Conclusion

In this paper, we have presented a tumor growth prediction framework which comprises a reaction-diffusion equation, a hyperelastic biomechanical model, a gradient-free nonlinear optimization algorithm, and physiological data fusion of structural and

functional image information. With the flexibility inherited from the gradient-free optimization, an objective function accounts for both ICVF MSE and tumor volume difference was proposed. Experiments on synthetic data show the importance of using the nonlinear biomechanical model and complementary measurements for model personalization. Experiments on clinical data show that the proposed framework can achieve promising prediction performance.

References

1. Bae, K.T.: Intravenous contrast medium administration and scan timing at CT: considerations and approaches. Radiology 256(1), 32–61 (2010)
2. Bathe, K.J.: Finite Element Procedures. Prentice Hall (1996)
3. Chen, X., Summers, R.M., Yao, J.: Kidney tumor growth prediction by coupling reaction-diffusion and biomechanical model. IEEE Transactions on Biomedical Engineering 60(1), 169–173 (2013)
4. Clatz, O., Sermesant, M., Bondiau, P.Y., Delingette, H., Warfield, S.K., Malandain, G., Ayache, N.: Realistic simulation of the 3D growth of brain tumors in MR images coupling diffusion with biomechanical deformation. IEEE Transactions on Medical Imaging 24(10), 1334–1346 (2005)
5. Fung, Y.C.: Biomechanics: Mechanical Properties of Living Tissues, 2nd edn. Springer (1993)
6. Hogea, C., Davatzikos, C., Biros, G.: An image-driven parameter estimation problem for a reaction-diffusion glioma growth model with mass effects. Journal of Mathematical Biology 56(6), 793–825 (2008)
7. Holzapfel, G.A.: Nonlinear Solid Mechanics: A Continuum Approach for Engineering. John Wiley & Sons, Inc. (2000)
8. Kormano, M., Dean, P.B.: Extravascular contrast material: the major component of contrast enhancement. Radiology 121(2), 379–382 (1976)
9. Liu, Y., Sadowski, S.M., Weisbrod, A.B., Kebebew, E., Summers, R.M., Yao, J.: Multimodal image driven patient specific tumor growth modeling. In: Mori, K., Sakuma, I., Sato, Y., Barillot, C., Navab, N. (eds.) MICCAI 2013, Part III. LNCS, vol. 8151, pp. 283–290. Springer, Heidelberg (2013)
10. Rowan, T.: Functional Stability Analysis of Numerical Algorithms. Ph.D. thesis, University of Texas at Austin (1990)
11. Stylianopoulos, T., Martin, J.D., Chauhan, V.P., Jain, S.R., Diop-Frimpong, B., Bardeesy, N., Smith, B.L., Ferrone, C.R., Hornicek, F.J., Boucher, Y., Munn, L.L., Jain, R.K.: Causes, consequences, and remedies for growth-induced solid stress in murine and human tumors. Proc. Natl. Acad. Sci. USA 109(38), 15101–15108 (2012)
12. West, G.B., Brown, J.H., Enquist, B.J.: A general model for ontogenetic growth. Nature 413(6856), 628–631 (2001)